Potential Energy Surface of the $\tilde{A}$ State of NH_2 and the Role of Excited States in the $N(^2D) + H_2$ Reaction

Lisa A. Pederson and George C. Schatz*

Department of Chemistry, Northwestern University, Evanston, Illinois 60208-3113

Timothy Hollebeek, Tak-San Ho, and Herschel Rabitz

Department of Chemistry, Princeton University, Princeton, New Jersey 08544-1009

Lawrence B. Harding

Chemistry Division, Argonne National Laboratory, Argonne, Illinois 60439

Received: July 19, 1999; In Final Form: October 5, 1999

We present a global potential energy surface for the $\tilde{A}$ state of NH_2 ($1^2A'$) based on application of the reproducing kernel Hilbert space (RKHS) interpolation method to high-quality ab initio (multireference configuration−interaction) results. This surface correlates adiabatically to the $a^1\Delta$ state of NH, with a reaction endoergicity of about 8 kcal/mol, but it can also lead to formation of ground-state NH (exoergic by 29 kcal/mol) via nonadiabatic (Renner−Teller) interactions for linear HNH geometries that lie near the bottom of a 94 kcal/mol deep well that is accessible from $N(^2D) + H_2$ by insertion over a 3.4 kcal/mol barrier. This insertion barrier is about 1 kcal/mol higher in energy than the corresponding insertion barrier associated with the ground state of $NH_2(1^2A'')$. As a result, the $\tilde{A}$ state contributes measurably to both the thermal rate constant for $N(^2D) + H_2$ and the rate for $NH(a^1\Delta)$ production. Extensive quasiclassical trajectory calculations are performed on the RKHS surface to study the $N(^2D) + H_2$ reaction dynamics, with the nonadiabatic rate constant estimated using a capture model. We find that the cross section for ground-state NH production is comparable to that obtained on the ground-state $1A''$ surface, except for a 1 kcal/mol shift upward in the effective threshold due to the different barrier height. The cross section for $NH(a^1\Delta)$ production has a higher threshold energy and is about 15% of the ground-state cross section at energies well above threshold.

I. Introduction

The reaction $N(^2D) + H_2\ (X^1\Sigma_g^+) \rightarrow NH(X^3\Sigma^-) + H(^2S)$ has been of significant interest in the past few years.[1−10] This reaction is the simplest of reactions involving the lowest excited state of nitrogen, and as such it plays a role in the chemistry of nitrogen containing fuels and of nitrogen in the atmosphere.[1] Early time-resolved spectroscopy work by Dodd and co-workers[2] provided evidence that this reaction produces inverted vibrational distributions that would be expected from a direct hydrogen atom abstraction mechanism. These conclusions were supported by subsequent theoretical studies based first on LEPS surfaces[3] and then on an ab initio (first-order configuration interaction (FOCI)) potential surface for the ground state reported by Kobayashi et al.[4] (hereafter denoted KTYST). In the KTYST work, it was found that the collinear (abstraction) reaction path was dominant in the reaction dynamics, and both trajectory[4] and quantum scattering[5] methods demonstrated the existence of inverted vibrational distributions. In the ab initio calculations, it was noted that there was also a perpendicular insertion reaction path, but this had a higher barrier than the collinear path (4.9 vs 1.3 kcal/mol) and thus was not important for thermal reagent energies.

In subsequent experimental and theororetical work, it was found that the earlier conclusions were incorrect. First, the laser-induced fluorescence studies of Umemoto and co-workers[5,7] demonstrated that the nascent vibrational distributions have $NH(\nu'' = 1)/NH(\nu'' = 0) = 0.8 \pm 0.1$ and $ND(\nu'' = 1)/ND(\nu'' = 0) = 1.0 \pm 0.1$, indicating little or no population inversion. Also, a crossed molecular beam (CMB) study of $N(^2D) + D_2$ by Alagia et al.[9] yielded a forward−backward symmetric product angular distribution at collision energies of 3.8 and 5.1 kcal/mol, which is indicative of insertion dynamics. This conclusion received further support from theoretical work by Pederson et al.,[10] who developed a new theoretical potential surface for the NH_2 ground-state based higher level ab initio calculations (second-order configuration interaction (SOCI)). This surface indicated a lower barrier for insertion to form NH_2 complexes rather than for direct abstraction, which is the opposite of what was found in the FOCI surface. Quasiclassical trajectory (QCT) calculations therefore gave nearly symmetric angular distributions[9] and nearly statistical vibrational distributions[10] which matched well with the most recent experiments. As a followup to their earlier theoretical work, Kobayashi and co-workers[8] studied the effect of varying the ratio of collinear and perpendicular barriers on their FOCI surface and found that reversing the order of these barriers produces a dramatic change in the product vibrational and angular distributions, corresponding to a change from abstraction to insertion dynamics that is similar to what is seen with the SOCI surface.

One aspect of the $N(^2D) + H_2$ reaction dynamics that has not been considered is the role of excited electronic states. There are five doublet states that correlate to $N(^2D) + H_2$ and one of

* To whom correspondence should be addressed.

10.1021/jp9924575 CCC: $19.00
Published on Web 11/19/1999

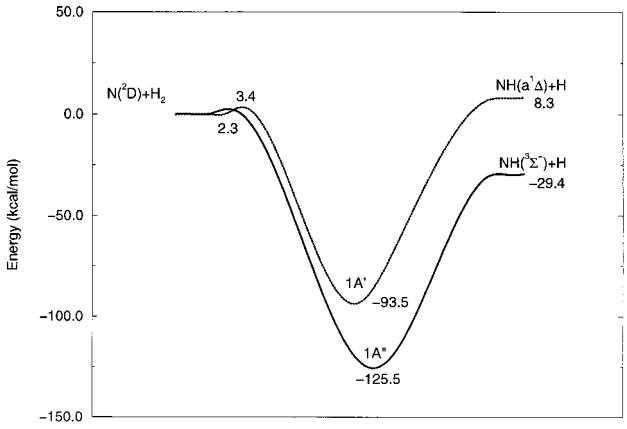

Figure 1. Schematic of the 1A′ and 1A″ potential surfaces for NH_2, showing the energies along the C_{2v} approach from the $N(^2D) + H_2$ reactants to the bottom of the NH_2 well and from the bottom of the well along the minimum energy path (not C_{2v}) to products. The energies given are based on the electronic structure calculations reported in this paper.

the excited states, the $\tilde{A}$ ($1^2A'$) state of NH_2, could be important. Figure 1 shows schematically what the minimum energy path between reagents and products looks like for this state and for the ground state. Although only the ground $1^2A''$ state correlates to the ground $^3\Sigma^-$ state of NH, the $\tilde{A}$ state, which correlates adiabatically to the $a^1\Delta$ state of NH, interacts with the ground state for linear HNH geometries, where these two surfaces form a degenerate Renner−Teller coupled pair having $^2\Pi$ symmetry. Such an intersection is qualitatively different from a conical intersection in that the energy difference between the two surfaces has a stronger than linear dependence on coordinates that break the degeneracy. However, like a conical intersection, the "seam" of intersection is a one-dimensional curve in the three-dimensional space that describes the potential surface. The lowest energy associated with the intersection seam lies ∼90 kcal/mol below the $N(^2D) + H_2$ reactants, so if this can be accessed from the reactants at energies that are not much higher than the ground-state barrier, then crossing to the ground state should be efficient, and the $\tilde{A}$ state would contribute significantly to the thermal reaction rate and to cross sections for ground-state production. In addition, this surface would also play a role in collisions that start off in the ground state by increasing the density of states accessible to the NH_2 intermediate. This should prolong its lifetime. Finally, this surface is responsible for the production of NH ($a^1\Delta$), which is also a measurable species in some experiments.

In this paper, we present extensive ab initio results for the $\tilde{A}$ state of NH_2 at a level that is comparable to our earlier work with the ground state. We also present a fit to the surface using the RKHS method and trajectory calculations of the reaction dynamics, which are used to estimate the cross sections and rate constants for producing ground and excited NH_2. This surface is also of relevance to studies of the $\tilde{A}$ state spectroscopy of NH_2, which is a subject with a rich history,[11] but we will not pursue this application here.

Section II presents the determination of the potential energy surface. Section III describes the quasiclassical trajectory calculations. Section IV provides the results and discussion, and Section V presents conclusions.

II. Potential Energy Surface

A. Electronic Structure Calculations. There are five surfaces that correlate to $N(^2D) + H_2$ ($X^1\Sigma_g^+$). For linear NHH geometries, these become $^2\Sigma^-$,$^2\Pi$, and $^2\Delta$ states and the $^2\Sigma^-$ surface, which is $1^2A''$ for C_s symmetry, has the lowest energy. The lowest excited state is the $1^2A'$ component of the $^2\Pi$ state, and it is this state that we will consider in this paper. As an abbreviation, we use the notation 1A″ or GS for the $1^2A''$ ground state and 1A′ or ES for the $1^2A'$ excited state.

The electronic structure results reported here come from multireference configuration interaction (MR−CI) calculations employing the Dunning augmented polarized triple-ζ (aug-pvtz) basis set.[12] In these calculations, the orbitals are first optimized using a seven active orbital, nine active electron, complete active space, multiconfiguration, self-consistent field wave function. For the subsequent MR−CI calculations, the reference space is reduced to six active orbitals and seven active electrons (the nitrogen 1s orbital is kept doubly occupied). The final CAS + 1 + 2, CI calculations then include all single and double excitations of the seven active valence electrons into the full virtual orbital space. The effects of higher-order excitations (beyond singles and doubles) have not been included in the present calculation, but they were studied in our earlier work[10] using the normalized Davidson correction,[13] and it was found that they only produce a small (0.5 kcal/mol) shift in the insertion barrier height. (The effect of a shift of this magnitude in the 1A′ surface on the comparisons between theory and experiment will be discussed later.) The calculations were carried out on an IBM-SP computer using the COLUMBUS program package,[14] and they required about 50 min per point, using IBM P2SC nodes (480 MFLOPS peak speed). A total of 1512 points on the 1A′ surface were calculated on a 12 × 18 × 7 3D grid (defined in ref 10) using a coordinate system where $R_1 = NH_1 + NH_2 - HH$, $R_2 = HH$, and $R_3 = (NH_1 - NH_2)^2/HH^2$. Here, NH_i and HH represent the N−H and H−H bond distances, respectively.

B. Constructing the NH_2 Potential. As with the studies on the H_2O surface,[15,16] the potential was determined from a many-body expansion:

$$V_{NHH}(R_1,R_2,R_3) = V^{(1)} + V^{(2)}_{NH}(R_1) + V^{(2)}_{NH}(R_2) + V^{(2)}_{HH}(R_3) + V^{(3)}_{NHH}(R_1,R_2,R_3)$$

where R_1, R_2, and R_3 are the diatomic N−H, N−H, and H−H bond distances respectively, and $V^{(1)}$, $V^{(2)}$, and $V^{(3)}$ are the one-, two-, and three-body terms. The one-body term is assigned the value of the dissociation energy in the three-atom limit $2H(^2S) + N(^4S)$. The two-body terms are determined from an interpolation of a discrete set of ab initio data points, $V^{(2)}_{NH}(R_1^i)$, $i = 1, ..., N_{R1}$, $V^{(2)}_{HH}(R_3^j)$, $j = 1, ..., N_{R2}$ etc. The three-body term is obtained by interpolating the difference between the ab initio data points and the corresponding one- and two-body sum

$$V^{(1+2)}_{NHH}(R_1,R_2,R_3) = V^{(1)} + V^{(2)}_{NH}(R_1) + V^{(2)}_{NH}(R_2) + V^{(2)}_{HH}(R_3)$$

on a 3D regular grid that is identical to that used in ref 10 for the 1A″ state. As in earlier papers on the H_2O system,[15,16] we used the reproducing kernel Hilbert space method[17] (RKHS) to do the interpolations. Some modifications that were implemented in the present application are described elsewhere.[18] A previous study on the $O(^1D) + H_2 \rightarrow OH + H$ system[15] demonstrated the accuracy and efficiency of the reproducing kernel Hilbert space fitting on a grid of only 1280 ab initio data points. In that application, the rms error was 0.3 kcal/mol for energies within 200 kcal/mol of the H_2O minimum. We have not determined the fitting error in the present study, but we expect that the surface should be of comparable accuracy.

III. Quasiclassical Trajectory Calculations

Quasiclassical trajectory (QCT) methods were used to study the $N(^2D) + H_2/D_2$ reaction on the 1A′ surface to make estimates of cross sections for forming both ground and excited NH. The excited-state cross section was obtained from the trajectories without any modification to the QCT procedure. To obtain the ground-state cross section, we have assumed a capture model, wherein any collision for which the potential energy at some point in the trajectory drops below half the NH_2 well depth is assumed to react to give ground-state NH + H. This model therefore assumes that trajectories that sample the lower half of the NH_2 well will eventually jump to the ground state and never return. This assumption is consistent with experience in studies of the A state of $O(^1D) + H_2$, which like the Ã state of $N(^2D) + H_2$, has an intersection seam with the ground state near the bottom of the initially formed well.[15] Trajectory surface hopping studies[19] as well as quantum dynamics studies[20,21] show that the hopping probability from the A state well in $O(^1D) + H_2$ to the ground state is in the range 50−100%. In the case of $N(^2D) + H_2$, the well is much deeper, which should enhance its lifetime and presumably enhance the chance for downward transitions. The choice of half the well depth is somewhat arbitrary; however it provides a measure of whether complex formation has occurred that has been used in past studies of $O(^1D) + H_2$, and it is still above the energy of the most accessible regions of the intersection seam between the two surfaces. Furthermore, the precise cutoff used is not very important, as trajectories that form complexes typically have very chaotic vibrational motions and end up sampling points near the bottom of the well within the first few vibrational periods. One point of uncertainty concerning this capture model is that the mechanism for nonadiabatic transitions is different than in $O(^1D) + H_2$, involving Renner−Teller interaction rather than electrostatic interaction, so we cannot be certain that the hopping probability is as large as is found in $O(^1D) + H_2$. In this respect, the capture model cross sections that we have determined provide an upper bound to the true Ã state cross sections, as a hopping probability of less than unity will tend to reduce the reactive cross section compared to what we would estimate. However, even if all we have is an upper bound, the result is still useful in determining how important the Ã state is in determining cross sections and rate constants.

A maximum impact parameter b_{max} of 3.0 a_0 was used for low energies (below 4 kcal/mol) increasing to 4.0 a_0 at higher energies. These small values of b_{max} are a reflection of the presence of a barrier to reaction, and they are in strong contrast to the much larger values needed to converge the cross sections for $O(^1D) + H_2$. The initial atom−diatom separation was chosen to be 10 a_0 for all calculations. A fifth-order Adams−Moulton predictor−corrector method was used for the trajectory calculations, using a time step of 0.1 fs.

The calculations have considered H_2 and D_2 in initial states $v = 0$, $J = 0$, 1, 2. For the calculation of rate constants, we have used the $J = 0-2$ results to determine the rotational Boltzmann averages. A total of 10 000 trajectories were evaluated for each energy and each reagent state with initial relative translational energies ranging from 2 to 10.0 kcal/mol. Thermal rate constants for the 1A′ state were determined by a numerical quadrature of the cross sections, and these were combined with 1A″ results that were reported previously[10] using a statistical weighting factor of 1/5 to account for the electronic degeneracy of each state.

To characterize the reaction mechanism, the results of trajectory calculations were analyzed with respect to the angle of approach of the $N(^2D)$ atom relative to the H_2 axis. This angle was defined for each reactive trajectory when the Jacobi separation coordinate $R(N-H_2)$ first reaches 4.0 a_0. The resulting cross sections were tabulated into 10° bins according to the value of the Jacobi angle, with 0° representing a collinear approach direction.

IV. Results and Discussion

A. Potential Energy Surface. Geometries, energies, and harmonic frequencies of the H_2 reagent, the NH product, and stationary points on the NH_2 fitted surface are given in Table 1. Experimental results that are not taken from ref 10 are taken from refs 22−25. Three columns of ab initio results are presented, with the first referring to the present 1A′ surface, without Davidson correction, the second to the 1A″ surface with Davidson correction (DC), and the third to 1A″ without Davidson correction. The fourth column contains a variety of experimental results that can be compared to the 1A′ and 1A″ results.

The table shows that the 1A′ surface has many of the same topological features as 1A″, with a lower barrier for the C_{2v} approach than for $C_{\infty v}$ and a minimum for the C_{2v} approach that lies well below the reagent and product asymptotes. In addition, we note that the $C_{\infty v}$ barrier has two imaginary frequencies on both surfaces, with the lower of these corresponding to bending motion at the linear barrier. This indicates that the linear barrier is not really a saddle point, and there is no well-defined linear reaction path. This point was discussed for the 1A″ surface in some depth.[10]

To compare 1A′ and 1A″ stationary point energies, we consider the 1A″ results without Davidson correction in Table 1. The table shows that the C_{2v} barrier is 1.1 kcal/mol higher on 1A′, while the linear barriers differ by 10.8 kcal/mol. This means that the 1A′ surface favors reaction through perpendicular geometries even more than its ground-state counterpart. The 1A′ surface correlates to the $a^1\Delta$ state of NH, which lies 8.3 kcal/mol above the ground state, so there is a question as to whether the collinear barrier for that surface determines the reactive threshold energy. However, as mentioned above, the linear barrier is unstable with respect to bending, so there must be a lower-energy bent reaction pathway. In fact, we will show later that there is no barrier for H + NH ($a^1\Delta$) addition to form $NH_2(1A')$, so the threshold energy for forming $NH(a^1\Delta)$ is just the reaction endoergicity.

Comparisons with experiment, which can be done for the reagents, the products, and the NH_2 intermediate, provide an indication of the accuracy of the calculations. The results in Table 1 show excellent agreement between theory and experiment for geometrical properties (bond distances and angles) for both surfaces. For the relative energies of the different stationary points, we note that for the 1A′ surface there is a 1.3 kcal/mol error in the reaction endoergicity and a −1.2 kcal/mol error in the depth of the NH_2 well. These errors are a little larger than for the corresponding 1A″ properties (no DC), but applying the Davidson correction to 1A″ makes the agreement poorer and comparable in quality to what we found for the 1A′ surface. The only one of these energy errors that could influence the results is the endoergicity associated with formation of $NH(a^1\Delta)$, as this determines the threshold for reaction. The zero-point corrected threshold should be at 5.4 kcal/mol, but the ab initio calculations predict 6.7 kcal/mol. We will correct for this error in making estimates of the thermal rate constant for forming $NH(a^1\Delta)$.

As a test of convergence of the 1A′ surface, we did two additional calculations of the $NH(a^1\Delta)$ energy, one including

TABLE 1: Stationary Point Properties of NH_2 (1A′ and 1A″) Potential Surfaces[a]

reaction/ property	1A′ (no DC) (present)	1A″ (DC) (ref 10)	1A″ (no DC) (ref 10)	experimental (ground state)	
$N(^2D) + H_2$					
energy	0	0	0	0	
R(H−H)	1.40	1.40	1.40	1.40	
frequency		4444	4461	4395	
NH + H	NH($a^1\Delta$)	NH($X^3\Sigma^-$)	NH($X^3\Sigma^-$)	NH($X^3\Sigma^-$)	($a^1\Delta$)
energy	8.3	−28.9	−29.4	−29.4	7.0[b]
R(N−H)	1.96	1.97	1.96	1.96[c]	1.97[d]
frequency	3311	3248	3287	3283[c]	3186[d]
H−H−N linear barrier					
energy	4.61	5.46	5.46		
R(N−H)	2.95	2.88	2.88		
R(H−H)	1.48	1.54	1.54		
frequencies	2184*i*, 914*i*, 1612	1015*i*, 447*i*, 3014	1067*i*, 487*i*, 2264		
C_{2v} barrier					
energy	3.39	1.93	2.29		
R(N−CM)	3.70	4.05	4.15		
R(H−H)	1.42	1.41	1.41		
frequencies	558*i*, 446, 4218	513*i*, 89, 4291	394*i*, 50, 4326		
	$^2A_1$	$^2B_1$	$^2B_1$	$^2B_1$	$^2A_1$
C_{2v} minimum					
energy	−93.5	−126.4	−125.5	−124.5	−92.3[e]
R(N−CM)	0.60	1.21	1.22	1.21	0.58[f]
HNH angle (deg)	142.7	102.7	102.4	103.0	144.2[f]
frequencies	3912, 3615, 1056	3445, 3347, 1514	3424, 3329, 1482		

[a] All energies are in kcal/mol, distances in a_0 and frequencies in cm^{-1} [b] This can be derived from ref 22, after zero point effects are removed. [c] Reference 23. [d] Reference 24. Similar results are noted in ref 22. [e] Based on T_o from ref 25 and zero point energy differences from the present theoretical calculations. [f] Reference 25.

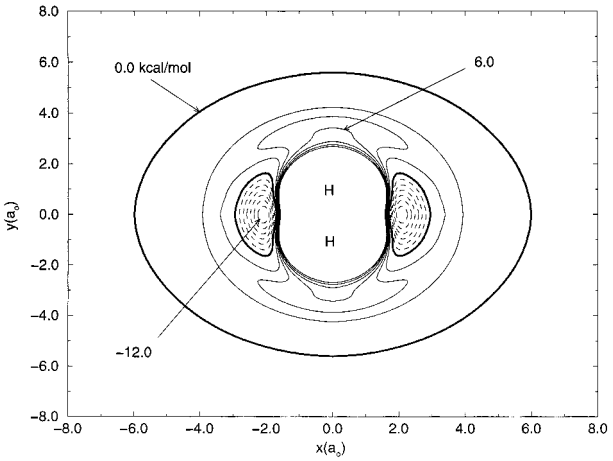

Figure 2. Contour plot of the 1A′ NH_2 potential as a function of the *x*, *y* location of the N atom with the HH bond distance fixed at 1.4 a_0 and oriented along the *y* axis. Contours are spaced by 2 kcal/mol; solid curves are used for energies that are positive relative to $N(^2D) + H_2$, dashed curves are used for energies which are negative, and a thick solid line denotes the zero energy contour.

the Davidson correction and the second increasing the basis set from aug-pvtz to aug-pvqz. We find that including for DC decreases the endoergicity by 0.6 kcal/mol while increasing the basis set also decreases the endoergicity by 0.6 kcal/mol. When both effects are included, the endoergicity is decreased by 1.2 kcal/mol, dropping it from 6.7 kcal/mol to 5.5 kcal/mol, which is only 0.1 kcal/mol above the experimental value.

Figure 2 presents a contour plot of the NH_2 (Ã) potential for a fixed HH distance of 1.4 a_0, as a function of the N atom coordinates. This shows the C_{2v} barrier and NH_2 well, although we note that the well depth (12 kcal/mol) is smaller than the full NH_2 well depth (93.5 kcal/mol) that is obtained if the HH distance is optimized. We also note the absence of a reaction path for collinear approach.

Figure 3 shows contours of the 1A′ potential for linear and perpendicular geometries and compares them with the corresponding result for the ground state (1A″) surface, which in this case was chosen to be the Davidson corrected surface from ref 10. These figures show the two stationary points that correspond to linear and perpendicular barriers, and the perpendicular geometry plots show the NH_2 minima. Note also that the line $R = 0$ in the perpendicular geometry plots refers to linear HNH configurations where the 1A′ and 1A″ surfaces should be degenerate. This degeneracy is only approximately present in the present figures for two reasons. One is that the 1A′ surface has not been Davidson corrected, so the underlying electronic structure data are of slightly different accuracy. The second is that the RKHS interpolation does not impose degeneracy for linear geometries into the kernel used in the fit. Both of these points are of minor significance for the present application where we are not explicitly coupling the two surfaces in dynamics calculations. However, in studies where the two surfaces are coupled it will be important to use a consistent electronic structure model and to use interpolation functions which force degeneracy for linear geometry.

Figure 4 shows contours of the potential for a fixed NH distance (equal to that in the separated diatomic) as a function of the H atom location. This shows the broad NH_2 well with its slightly nonlinear minimum. There is no apparent barrier to H + NH addition along a path in which the H atom approaches almost perpendicularly to the NH bond. This means that the activation energy for reaction on the 1A′ surface to produce NH($a^1\Delta$) + H will be equal to the reaction endoergicity. The figure also shows a repulsive bump (due to a conical intersection), corresponding to linear HNH geometries, and more globally repulsive regions for linear NHH geometries.

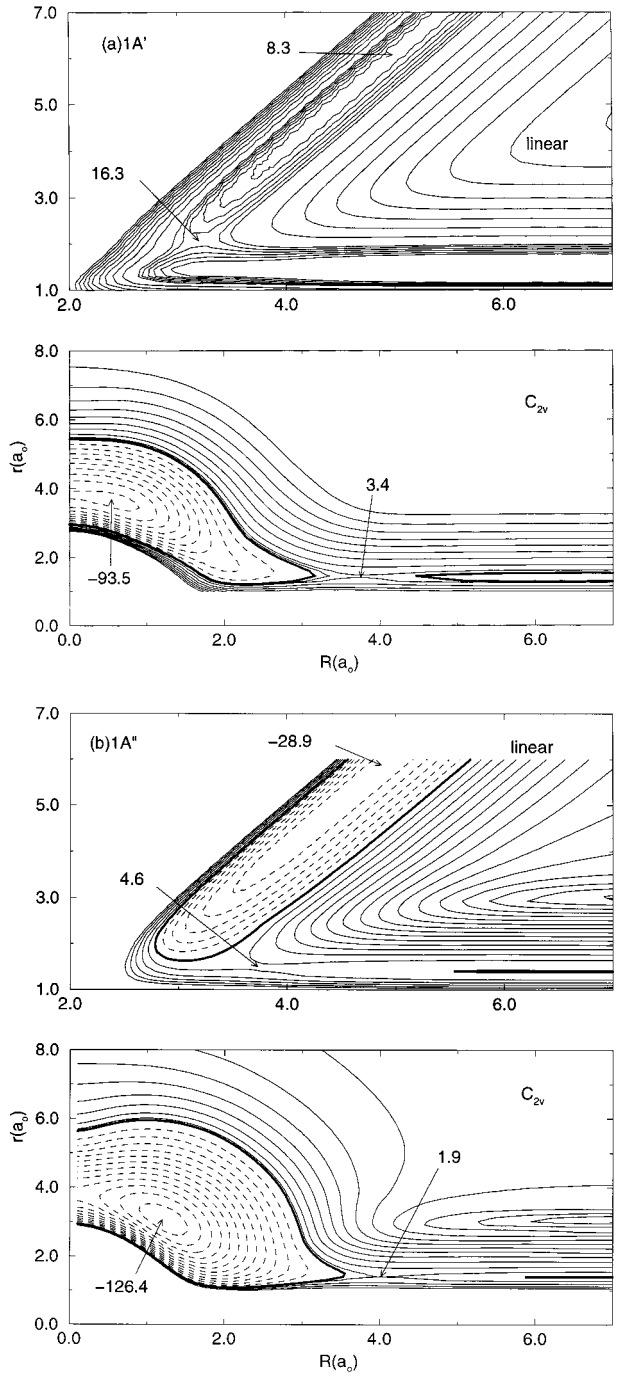

Figure 3. Contour plot of the NH_2 potential for the (a) 1A′ and (b) 1A″ states. The 1A″ surface is the Davidson corrected surface that was reported in ref 10. For both surfaces, the potential is plotted as a function of the Jacobi coordinates *R* (N to HH center of mass distance) and *r* (HH distance), with the top panel showing linear configurations and the bottom perpendicular configurations. Contours are spaced by 2 kcal/mol for positive energy contours (solid curves) and 10 kcal/mol for negative energy contours (dashed) with the zero-energy contour (defined as $N(^1D) + H_2$ at equilibrium) denoted by a thick solid line.

B. Integral Cross Sections. Figure 5 presents the integral cross section as a function of reagent kinetic energy for $N(^2D) + H_2$ ($v = 0, j = 0$). The cross sections refer to the 1A″ ground state (GS) and the 1A′ excited state (ES) using the adiabatic surface and using the capture model (ES capture) estimate (i.e., trajectories dropping below half the well depth assumed to hop to the lower surface with 100% probability). We also show the sums of ground- and excited-state cross sections, as these would be important in determining thermal rate constants.

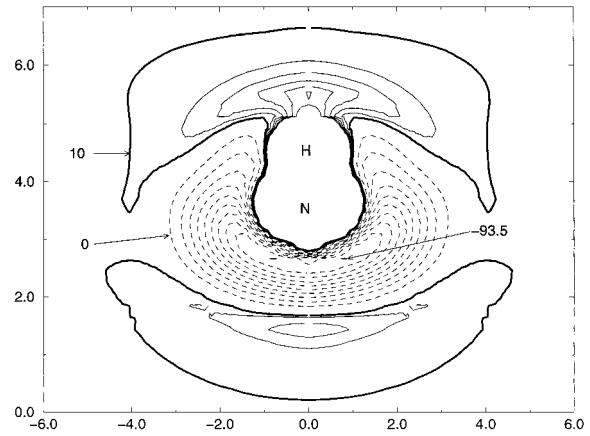

Figure 4. Contour plot of the 1A′ surface, analogous to Figure 2 but with the NH bond fixed at 1.97 a_0 and the H atom location variable. The contour spacing is 10 kcal/mol, and the energy zero is chosen to be $N(^2D) + H_2$ at equilibrium, so the $H + NH(a^1\Delta)$ asymptote is at 8.3 kcal/mol and the $NH_2(^2A_1)$ minimum is at −93.5 kcal/mol.

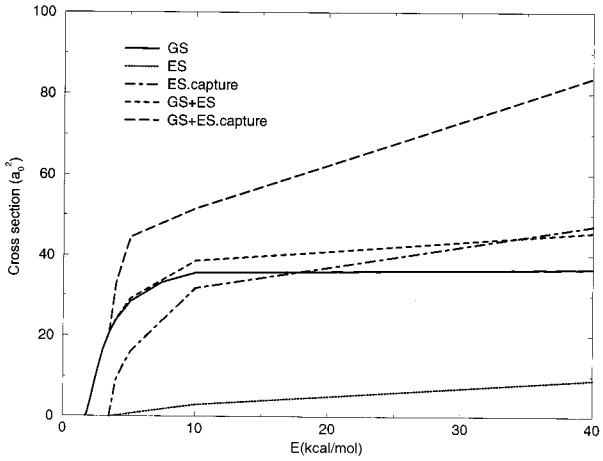

Figure 5. Integral cross section (a_0^2) versus energy (kcal/mol) for $N(^2D) + H_2$ ($v = 0, j = 1$), including results for the 1A″ ground-state surface (GS), the 1A′ excited state to produce excited products (ES), the 1A′ excited state estimate to produce ground-state products based on the capture model (ES.capture), the sum of 1A′ + 1A″ (GS + ES), and the sum of 1A′ + 1A″ to produce ground-state products (GS + ES.capture).

The figure shows that the ground-state cross section has an effective threshold of slightly less than 2 kcal/mol, while the excited state (capture model) has a threshold of about 3.5 kcal/mol. Both threshold energies are similar in value to the corresponding C_{2v} barrier energies (1.9 and 3.4 kcal/mol, respectively). Above threshold, the cross sections have a similar dependence on translational energy, and well above threshold they have similar magnitudes as well. This suggests that, except for the difference in barrier height, the two surfaces are similar in the entrance channel region near the barrier top.

The cross section for production of excited-state products ($NH(a^1\Delta) + H$) has a threshold energy of about 4 kcal/mol and is much smaller than the capture model cross section at energies well above threshold. This threshold energy is lower than the zero-point corrected endoergicity (6.7 kcal/mol) due to zero-point energy violation (i.e., NH_2 complexes decay to $NH(a^1\Delta) + H$ with the NH having less than zero-point energy). We could correct the trajectories for this error by omitting trajectories with less than zero-point energy, but since there is also an error in the threshold due to the ab initio results, we have chosen instead to simply shift the cross sections to correct for both errors in computing rate constants (see below). The small cross section

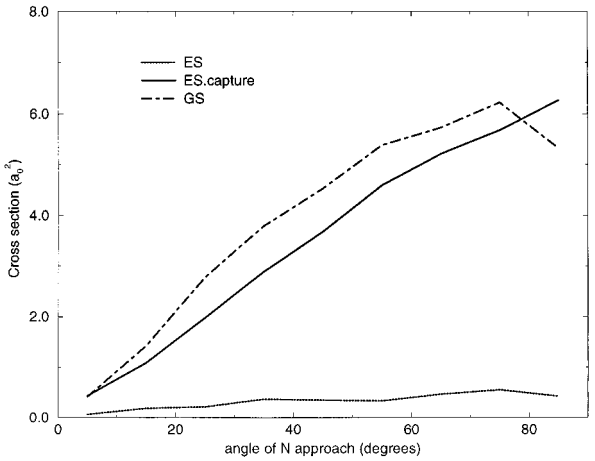

Figure 6. Contribution to the integral cross section from different angles of approach for GS, ES, and ES.capture (see Figure 5 for explanation of notation). The translational energy is 10 kcal/mol, and the initial state of $N(^2D) + H_2$ is $v = 0$, $j = 1$.

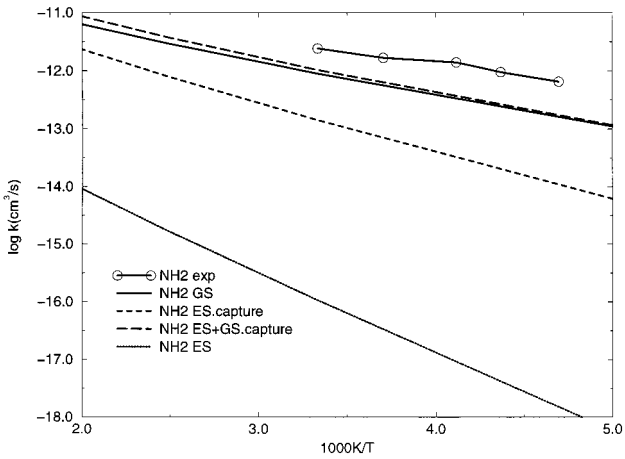

Figure 7. Thermal rate constants (cm^3/s) for $N + H_2$ for GS, ES, and ES.capture, and for the sum GS + ES.capture, plotted as an Arrhenius plot. Experimental data from ref 3 are also included in the plot.

for $NH(a^1\Delta)$ production, which is only about 15% of the capture model estimate, even at energies well above threshold, is what one might expect for a largely statistical decay of the intermediate NH_2 complex, as this can decay over a lower barrier back to the reactants than to products.

To study the mechanism of reaction, in Figure 6 we present the cross section versus angle of approach of N relative to H_2 at a translational energy of 10 kcal/mol for the GS, ES, and ES.capture results. The angle of approach was defined in ref 10 as the angle between the Jacobi R and r vectors at a point where the R first decreases below 4 a_0. Thus, an angle of 90° corresponds to perpendicular approach of the N to the H_2, and we see that the largest reactivity for all three mechanisms arises for angles close to this. This is what would be expected, given that this is the lowest-energy reaction path. Both ES and ES.capture cross sections show a similar dependence on approach angle, which is the expected result for processes where the entrance channel bottleneck determines the reactivity.

In ref 10, we examined product state information, including angular, vibrational, and rotational distributions, for the ground-state surface. It is not possible to use the capture model to determine this information for the reaction that starts in the excited state, but there is every reason to believe that the results will be similar to the ground-state results. We can, however, determine $NH(a^1\Delta)$ vibrational and rotational distributions. Since this channel is endoergic, the vibrational and rotational distributions are much colder, with only $NH(v = 0)$ produced for energies close to threshold and rotational distributions that are largely statistical. We omit giving further details, as there are no experiments to compare them with.

C. Thermal Rate Constants. Figure 7 presents thermal rate constants for $N(^2D) + H_2$, plotted as an Arrhenius plot and compared with the results of experiment. Included in this plot are results based on all the results in Figure 5, including GS, ES, ES capture, and GS + ES.capture. In calculating the ES result, we have shifted the cross sections so that the threshold energy for formation of $NH(a^1\Delta)$ is at 5.4 kcal/mol. Also, the ES.capture cross sections have been shifted down 0.5 kcal/mol to provide an estimate of what the Davidson corrected cross section would be. The ES rate constants have been obtained by fitting the calculated integral cross sections in the 4−4.5 kcal/mol region to a straight line, then shifting to make the $j = 0$ threshold 5.4 kcal/mol and doing the appropriate average over a thermal distribution of energies. The rate constants are further averaged over a Boltzmann distribution of rotational states to produce the results in Figure 7. A similar procedure was used for ES.capture, except that the range of energies used was 3.5−4.0 kcal/mol.

The results in Figure 7 show that the GS calculated rate constants are systematically lower than experiment by about a factor of 2.7 for temperatures near 300 K. This point was discussed in ref 10, and it was suggested that this may be due to a combination of a barrier that is still too high and the absence of tunneling in the trajectory calculation. If all of the error were due to the barrier height, this would have to be reduced by about 0.6 kcal/mol to match experiment. Adding in the ES capture contribution reduces the error, but the ES.capture rate constant is only 12% of the GS result at 300 K, so the improvement is not significant. This is as one would expect, given that the ES barrier is 1 kcal/mol higher than GS.

No estimates of the rate constant for formation of $NH(a^1\Delta)$ have been made previously. Our results indicate that this rate constant is a factor of 10^4 smaller than the rate constant for forming ground-state products at 300 K.

V. Conclusions

We have obtained an analytical surface for the 1A′ state of NH_2 within the framework of the reproducing kernel Hilbert space theory based on high-level triple-ζ SOCI ab initio results. This surface shows that the $N(^2D) + H_2$ reaction dynamics in the lowest excited state is dominated by insertion. Insertion was also found for the ground state 1A″ surface, so since these two surfaces are the only ones with barriers that can be surmounted at thermal energies, we can conclude that insertion governs the thermal and low energy reaction dynamics for this reaction.

Classical trajectory calculations were performed for $N(^2D) + H_2$, and cross sections were determined from two dynamical models: a capture model that provides an estimate of the cross section for forming ground-state NH from excited state reactants by assuming that there is 100% probability for hopping to the ground state once trajectories reach at least halfway to the bottom of the excited state well, and a standard electronically adiabatic model that assumes that the excited and ground states are not coupled. The capture model indicates that the cross section for reaction in the excited state is very similar to that in the ground state, except for a shift in translational energy by the difference in barrier heights (roughly 1 kcal/mol). As a result, the excited state contributes to the thermal rate constant, especially at high temperatures. However, the calculated thermal

rate coefficients are still below experiment, which indicates that additional errors remain. Most likely this means that the barrier height on the ground-state surface is too high, but it is also possible that tunneling plays a significant role in the results. The cross section for producing $NH(a^1\Delta)$ is much smaller than the capture model cross section, amounting to only 12% of the capture cross section even at high translational energy. Also, the threshold for excited-state production is higher than the C_{2v} barrier energy, due to the fact that $NH(a^1\Delta)$ formation is endoergic starting from $N(^2D) + H_2$. This leads to rate constants for production of $NH(a^1\Delta)$ that are a factor of 10^4 below those for ground-state formation.

We have not computed final state distributions for the nonadiabatic reaction, as this would require doing a coupled surface calculation that includes Renner−Teller interactions between the 1A′ and 1A″ states. This will be a useful task for the future. However, it seems likely that the angular and internal state distributions that would be obtained from such a calculation will be very similar to what has already been generated for the 1A″ state in adiabatic calculations.

Acknowledgment. This work was supported by NSF Grant CHE-9527677(G.C.S., L.A.P.), the U.S. Department of Energy, Office of Basic Energy Sciences, Division of Chemical Sciences, under Contract No. W-31-109-ENG-38 (L.B.H.), and Contract No. DE-FG02-8GER13480 (T.H., T.S.H., and H.R.).

References and Notes

(1) Wright, A. N.; Winkler, C. A. *Active Nitrogen*; Academic Press: New York, 1968.

(2) Dodd, J. A.; Lipson, S. J.; Flanagan, D. J.; Blumberg, W. A. M.; Person, J. C.; Green, B. D. *J. Chem. Phys.* **1991**, *94*, 4301.

(3) Suzuki, T.; Shihira, Y.; Sato, T.; Umemoto, H.; Tsunashima, S. *J. Chem. Soc., Faraday Trans.* **1993**, *89*, 995.

(4) Kobayashi, H.; Takayanagi, T.; Yokoyama, K.; Sata, T.; Tsunashima, S. *J. Chem. Soc., Faraday Trans.* **1995**, *91*, 3771.

(5) Umemoto, H.; Matsumoto, K. *J. Chem. Phys.* **1996**, *104*, 9640.

(6) Takayanagi, T.; Kobayashi, H., Tsunashima, S. *J. Chem. Soc., Faraday Trans.* **1996**, *92*, 1311.

(7) Umemoto, H.; Asai, T.; Kimura, Y. *J. Chem. Phys.* **1997**, *106*, 4985.

(8) Kobayashi, H.; Takayanagi, T.; Tsunashima, S. *Chem. Phys. Lett.* **1997**, *277*, 20.

(9) Alagia, M.; Balucani, N.; Cartechini, L.; Casavecchia, P.; Volpi, G. G.; Pederson, L. A.; Schatz, G. C.; Lendvay, G.; Harding, L. B.; Hollebeek, T.; Ho, T.-S.; Rabitz, H. *J. Chem. Phys.* **1999**, *110*, 8857.

(10) Pederson, L. A.; Schatz, G. C.; Ho, T.-S.; Hollebeek, T.; Rabitz, H. *J. Chem. Phys.* **1999**, *110*, 9091.

(11) Dressler, K.; Ramsay, D. A. *Trans. R. Soc. London, Ser. A.* **1959**, *251*, 553. Brandi, R.; Leonardi, E.; Petrongolo, C. *J. Phys. Chem. A*, **1997**, *101*, 5696 and references therein.

(12) Dunning, T. H., Jr. *J. Chem. Phys.* **1989**, *90*, 1007. Kendall, R. A.; Dunning, T. H., Jr.; Harrison, R. J. *J. Chem. Phys.* **1992**, *96*, 6796. Woon, D. E.; Dunning, T. H., Jr. *J. Chem. Phys.* **1993**, *98*, 1358.

(13) Langhoff, S. R.; Davidson, E. R. *Int. J. Quantum Chem.* **1974**, *8*, 61. Silver, D. W.; Davidson, E. R. *Chem. Phys. Lett.* **1978**, *52*, 403.

(14) Shepard, R.; Shavitt, I.; Pitzer, R. M.; Comeau, D. C.; Pegger, M.; Lischka, H.; Szalay, P. G.; Ahlrichs, R.; Brown, F. B.; Zhao, J.-G. *Int. J. Quantum Chem.* **1988**, *S22*, 149.

(15) Ho, T.-S.; Hollebeek, T.; Rabitz, H.; Harding, L. B.; Schatz, G. C. *J. Chem. Phys.* **1996**, *105*, 10472.

(16) Schatz, G. C.; Papaioannou, A.; Pederson, L. A.; Harding, L. B.; Hollebeek, T.-S.; Rabitz, H. *J. Chem. Phys.* **1997**, *107*, 2340.

(17) Ho, T.-S.; Rabitz, H. *J. Chem. Phys.* **1996**, *104*, 2584.

(18) Hollebeek, T.; Ho, T.-S.; Rabitz, H. *Annu. Rev. Phys. Chem.* **1999**, *50*, 537.

(19) Pederson, L. A.; Schatz, G. C. *Faraday Discuss. Chem. Soc.* **1997**, *108*, 357.

(20) Drukker, K.; Schatz, G. C. *J. Chem. Phys.* **1999**, *111*, 2451.

(21) Gray, S. K.; Petrongolo, C.; Drukker, K.; Schatz, G. C. *J. Phys. Chem.*, in press.

(22) Berghout, H. L.; Brown, S. S.; Delgado, R.; Crim, F. F. *J. Chem. Phys.* **1998**, *109*, 2257.

(23) Martin, J. M. L. *Chem. Phys. Lett.* **1988**, *292*, 1411.

(24) Herzberg, G. *Molecular Spectra and Molecular Structure*; D. Van Nostrand Co.: Princeton, NJ, 1945; Vol. 1.

(25) Jungen, Ch.; Hallin, K.-E.; Merer, A. J. *Mol. Phys.* **1980**, *40*, 25.